

Satellite retrieval of inherent optical properties by inversion of an oceanic radiance model: a preliminary algorithm

Frank E. Hoge, C. Wayne Wright, Paul E. Lyon, Robert N. Swift, and James K. Yungel

A previously published radiance model inversion theory has been field tested by using airborne water-leaving radiances to retrieve the chromophoric dissolved organic matter (CDOM) and detritus absorption coefficient, the phytoplankton absorption coefficient, and the total backscattering coefficient. The radiance model inversion theory was tested for potential satellite use by comparing two of the retrieved inherent optical properties with concurrent airborne laser-derived truth data. It was found that (1) matrix inversion of water-leaving radiances is well conditioned even in the presence of instrument-induced noise, (2) retrieved CDOM and detritus and phytoplankton absorption coefficients are both in reasonable agreement with absorption coefficients derived from airborne laser-induced fluorescence spectral emissions, (3) the total backscattering retrieval magnitude and variability are consistent with expected values for the Middle Atlantic Bight, and (4) the algorithm performs reasonably well in Sargasso Sea, Gulf Stream, slope, and shelf waters but is less consistent in coastal waters. © 1999 Optical Society of America

OCIS codes: 010.3640, 010.4450, 280.3640, 300.6280.

1. Introduction

Present empirical radiance ratio algorithms¹ applied to satellite ocean color data provide an estimate of only the chlorophyll pigment and cannot properly account for the absorption and backscattering from other constituents including chromophoric dissolved organic matter (CDOM). Our object in this paper is to describe the results from field tests of a theory² for simultaneously retrieving three dominant inherent optical properties (IOP's) of water-leaving ocean radiance: the CDOM and detritus absorption, phytoplankton absorption, and total backscattering coefficients from satellite ocean color data by linear matrix inversion of a water-leaving radiance model. (Note that the *variable*, total constituent backscattering (TCB), is actually retrieved and the total backscattering is simply obtained by adding the *constant* backscattering coefficient of seawater.)

Radiance model inversion is tested using airborne

ocean color radiance spectra acquired during two missions flown under clear sky conditions. The performance of the algorithm is primarily evaluated using concurrent airborne laser-induced fluorescence data with a limited amount of supporting measurements made from samples acquired during a cruise of the University of Delaware Research Vessel (R/V) Cape Henlopen. Airborne laser-induced fluorescence data were chosen as the primary test set because of ready availability of large numbers of essentially paired active (laser-induced fluorescence) and passive ocean color radiance spectra and the previously demonstrated agreement between ship-derived chlorophyll and CDOM measurements. More than 7000 pairs of such active and passive spectra are acquired along ~450-km flight track in a single hour covering several different types of water masses. By comparison, ship data to support a similar radiance algorithm evaluation would require more than 24 h to traverse and would thus have considerable smearing because of advection and natural changes in the phytoplankton population. Moreover, the number of supporting ship samples would be far lower and statistically less robust.

At this stage of development, the algorithm is designated preliminary because (1) airborne laser-induced chlorophyll fluorescence data were used for

F. E. Hoge and C. W. Wright are with NASA, Wallops Flight Facility, Building N159, Wallops Island, Virginia 23337. P. E. Lyon, R. N. Swift, and J. K. Yungel are with EG&G, Incorporated, Wallops Flight Facility, Wallops Island, Virginia 23337.

Received 26 May 1998; revised manuscript received 22 September 1998.

phytoplankton absorption coefficient validation with only partial supporting ship observations of CDOM and chlorophyll; (2) the coastal zone retrievals are not as consistent as the shelf, slope, Gulf Stream, and Sargasso Sea retrievals; (3) the CDOM and detritus absorption coefficient is treated as a single IOP to reduce the required number of spectral bands; and (4) one of the three IOP's (backscattering coefficient) has not been validated.

The detailed theoretical development for linear matrix inversion of an oceanic radiance model has been given elsewhere.² The reader is urged to become familiar with the paper in Ref. 2 because much of the salient material is not repeated here.

2. Linear Matrix Inversion Methodology

There are many constituents within the ocean that contribute to upwelled spectral radiance, and any number of absorbers and backscattering components can in principle be retrieved. But for the preliminary algorithm presented in this paper, the principal constituents are assumed to be phytoplankton absorption, $a_{\text{ph}}(\lambda_i)$; CDOM and detritus absorption, $a_d(\lambda_i)$; and TCB, $b_{\text{bt}}(\lambda_i)$. It has been shown² that these three IOP's can be retrieved from the following matrix equation:

$$a_{\text{ph}}(\lambda_g)\exp[-(\lambda_i - \lambda_g)^2/2\sigma^2] + a_d(\lambda_d)\exp[-S(\lambda_i - \lambda_d)] + b_{\text{bt}}(\lambda_b)(\lambda_b/\lambda_i)^n v(\lambda_i) = h(\lambda_i), \quad (1)$$

where $h(\lambda_i) = -[a_w(\lambda_i) + b_w(\lambda_i)v(\lambda_i)]$ is the column matrix, or vector, of hydrospheric constants (seawater absorption and backscattering) and the oceanic water-leaving radiances. See Appendix A for the definitions of symbols. The $a_w(\lambda_i)$ and $b_w(\lambda_i)$ are seawater constants. Each of the IOP models for the chlorophyll absorption coefficient, the CDOM and detritus absorption coefficient, and the TCB have already been described.² The IOP model reference wavelengths λ_g , λ_d , and λ_b need not coincide with the sensor observational bands.² The matrix formulation of the radiance model inversion exemplified by Eq. (1) is a powerful framework for IOP retrievals as well as analysis of errors in the retrievals.² These error analyses² have shown that the accuracy of the CDOM and detritus absorption retrieved by linear inversion is strongly dependent on the accuracy of the exponent n in the TCB spectral model $b_{\text{bt}}(\lambda) = b_{\text{bt}}(\lambda_b)(\lambda_b/\lambda)^n$. Although we obtained reasonable inversions with a constant n value, better results are presently obtained if n is not held constant but allowed to vary with the constituent-driven radiances. Accordingly, the spatially variable n exponent³⁻⁶ should be varied to accommodate the different types of scattering constituents in the water masses under observation. We accomplished this by varying n based on a radiance ratio, L_1/L_3 , using two of the three bands being inverted. Numerous airborne active-passive⁷⁻⁹ data sets have shown that this ra-

diance ratio is linearly related to the exponent n such that

$$n = a_1 L_1/L_3 + a_2. \quad (2)$$

At the present stage of our algorithm approach we empirically derive n for each individual data set by experimentally minimizing the error in the retrieved CDOM and detritus coefficient compared with CDOM absorption derived from the laser-induced fluorescence measured with the NASA Airborne Oceanographic Lidar (AOL). For example, the best retrievals were found when the n factor algorithm for the 3 April 1995 inversions used a scale a_1 of 0.282 and an offset a_2 of 3.82 whereas the 20 April 1995 transects used an a_1 of 0.245 and an offset a_2 of 4.41. These values of a_1 and a_2 are not global, and other unpublished data sets have given optimal IOP retrievals with slightly different a_1 and a_2 values. The need to vary the n exponent would be eliminated if improved backscattering spectral models were available to better represent the diverse types of scatterers. Finding a single backscattering spectral model to represent a multitude of constituents requires empirical methods to fit the various combinations of these scatterers found in the global oceans.

Equation (1) is linear in the three IOP's at their reference wavelengths $a_{\text{ph}}(\lambda_g)$, $a_d(\lambda_d)$, and $b_b(\lambda_b)$. Three sensor wavelengths are required to provide an even-determined, consistent solution. The oceanic state vector of unknown IOP's at their reference wavelengths, $\mathbf{p} = [a_{\text{ph}}(\lambda_g), a_d(\lambda_d), b_b(\lambda_b)]^T$, where T denotes the transpose, is the solution of a matrix equation of the form $\mathbf{D}\mathbf{p} = \mathbf{h}$, where \mathbf{D} is the data model matrix and \mathbf{h} is the vector of seawater absorption and backscattering hydrospheric constants and radiance data.² It is important to emphasize that the \mathbf{D} matrix must be inverted for each radiance spectrum because it contains radiance data in addition to model parameters. It is potentially possible to extend the matrix inversion to a larger number of constituents as long as accurate IOP models can be found to satisfactorily represent the spectral absorption and backscattering of each (and sufficient sensor bands are available in the observational data to yield a solution). (The column vectors in the \mathbf{D} matrix can be reformulated so that the constants that represent the spectral models can be referenced to the first chosen sensor band wavelength λ_1 . This simplifies the matrix inversion and retrieves constituent IOP's as they exist at measured radiance wavelengths. Accordingly, an alternate form of the \mathbf{D} matrix has been given² together with suggestions for the derivation of constituent concentrations from the IOP state vector \mathbf{p} . Our preliminary algorithm in this paper focuses on even-determined solutions in which the number of IOP's (unknowns) is equal to the number of sensor bands (equations). In this case, the solutions, if obtainable, are unique. Future algorithm studies will address overdetermined least squares, weighted least squares, and other solutions.

3. Algorithm Validation with Airborne Laser Spectrofluorometry

A. Phytoplankton Absorption Coefficient Validation

In our analysis we utilized AOL laser-induced fluorescence measurements to validate retrieved IOP's. During the past ~13 years this technique proved valuable for testing algorithms for the retrieval of CDOM, chlorophyll, and potentially phycoerythrin from water-leaving radiance spectra. We corrected the laser-induced fluorescence measurements for variation in the surface layer attenuation properties by normalizing these backscattered signals with the concurrent laser-induced water Raman signal.¹⁰ Numerous comparisons have shown good agreement between airborne water Raman-normalized laser-induced chlorophyll fluorescence (F/R) measurements acquired with the AOL and ship-derived chlorophyll extraction measurements.^{7-9,11-15} Regressions between the extracted chlorophyll measurements and the AOL F/R values yielded a consistent F/R:μg/l conversion factor over various sections of the north Atlantic Ocean in spite of the known fluorescence and unit chlorophyll variability that was due to nutrient and phytoplankton physiology. The effects of light history are minimized by flying under clear skies near the middle of the day.

Because of (a) the high variability of the fluorescence per unit chlorophyll biomass and (b) the circuitous nature of biomass-to-absorption conversions, we use a more direct fluorescence-to-absorption conversion to provide a test data set to evaluate the retrieved phytoplankton absorption coefficient. There is strong evidence that the fluorescence per unit of phytoplankton absorption coefficient is constant across wide areas of the ocean surface layer. Specifically, for a 170-km distance a constant fluorescence-to-phytoplankton absorption coefficient provided remarkable agreement between observed water-leaving radiances and forward-modeled radiances whereas the chlorophyll biomass varied⁸ from 0.7 to 27 mg/m³. Thus we assume that the fluorescence per unit of phytoplankton absorption coefficient is constant across the entire experiment track lines. The laser-induced chlorophyll F/R ratios are converted to absorption values through equations of the form $F/R = k_0 [a_{ph}(412)]^{k_1}$ or $\exp\{\ln[(F/R)/k_0]/k_1\} = a_{ph}(412)$ where k_0 and k_1 are constants. Fluorescence per unit of phytoplankton absorption coefficient conversion factors is sometimes adjusted for different locations and dates to account for possible nutrient, light history, or species physiology. Accordingly, the parameters k_0 and k_1 were derived for each mission location and date to secure the best agreement with the passively retrieved phytoplankton absorption coefficient.

B. Chromophoric Dissolved Organic Matter and Detritus Absorption Coefficient Validation

Recently it was firmly established through ship and laboratory experiments that the absorption coefficient of CDOM is linearly related to the CDOM

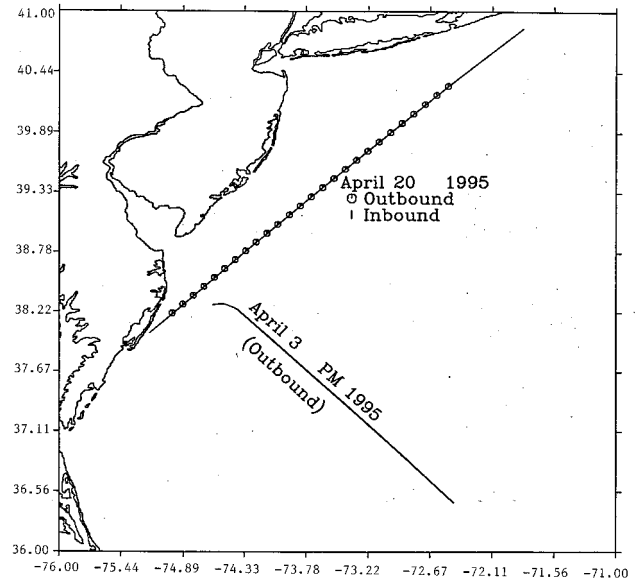


Fig. 1. Flight location of the AOL system and spectroradiometers aboard the NASA P-3B aircraft during the afternoon of 3 April 1995 is shown by the outbound southeast ground track line. This flight traversed five water masses: coastal, shelf, slope, Gulf Stream, and Sargasso Sea. Flight of the AOL system and spectroradiometers aboard the NASA P-3B aircraft on 20 April 1995 is shown by the outbound (toward the northeast) and inbound (toward the southwest) ground track lines. These latter track lines traversed only shelf and coastal water types.

fluorescence.¹⁶⁻¹⁹ Subsequently it was shown that the CDOM absorption coefficient IOP can be retrieved from airborne laser-induced and water Raman-normalized CDOM fluorescence in a variety of oceanographic locations.¹⁹ Because the detritus contributes little fluorescence to the airborne laser-induced fluorescence signal,^{16,19} the retrieved CDOM and detritus absorption coefficient will be only slightly larger than the airborne laser-derived CDOM absorption coefficient truth.

C. Total Backscattering Validation

No airborne laser system is presently available for the retrieval of the total backscattering coefficient. Thus no truth data are available for the TCB IOP. Furthermore, little backscattering data are available from ship cruises, perhaps because multiband instrumentation has only recently become available.³ The passively retrieved backscattering coefficient is consistent with noncontemporaneous determinations for the Middle Atlantic Bight.

4. Airborne Field Experiments in the Middle Atlantic Bight

Two airborne experiments conducted in the Middle Atlantic Bight (MAB) were selected for the purpose of testing the retrieval of IOP's from water-leaving radiances by radiance model inversion. Figure 1 shows a sampling line occupied during a flight on the afternoon of 3 April 1995 and by the University of Delaware R/V Cape Henlopen on 2 April 1995. The

complete outbound transect allows a stringent test of the algorithm because five different water masses were traversed: Sargasso Sea, Gulf Stream, continental slope, shelf, and coastal. (The inbound transect was not analyzed because other experiments were conducted during that portion of the flight.) To further test the algorithm in continental shelf and coastal waters, we selected an active-passive data set acquired during a flight conducted between Wallops Island, Virginia, and Block Island, Rhode Island, on 20 April 1995 as shown in Fig. 1. This latter flight was not supported by observations from a research vessel.

A. Passive (Solar) Data

A 256-channel ocean-viewing spectroradiometer was used to gather upwelled spectral radiance during the flights conducted from the NASA Goddard Space Flight Center P-3B aircraft. This spectroradiometer was set to provide spectral coverage between ~400 and 730 nm and was calibrated by viewing a Lab-sphere reflectance plaque illuminated by a National Institute of Standards and Technology (NIST) traceable irradiance standard lamp. The radiometer calibration was also checked for consistency by viewing an internally illuminated 0.75-m-diameter calibration sphere placed beneath the aircraft. This calibration sphere is similar to the one described by others.²⁰ The output radiance of the calibration sphere is also traceable to NIST sources. The sphere was a part of a sea-viewing wide field-of-view sensor intercalibration round-robin experiment (SIRREX)²¹ calibration activity. An AOL team member participated in a subsequent SIRREX forum to further enhance our knowledge of the characterization of the plaque and the sphere. The spectral calibration of the spectroradiometer is validated by viewing a Hg-Cd source. The spectroradiometer was found by repeated laboratory experiments to be at least as stable as the NIST traceable sources. When further tested against nonfilament radiance sources such as light-emitting diodes, the stability was likewise found to equal such sources. The field of view (~2 mrad) and integration time (~350 ms) yield a pixel size of ~0.3 m × 45 m for a flight speed of ~125 m/s of the P-3B aircraft. The radiometer pixels are located ~30° off nadir (port or starboard) to avoid Sun glint. (The 10-pulse/s laser footprints are each ~0.3 m in diameter but are located directly under the aircraft at 5° off nadir toward the nose of the aircraft. Thus the active and passive pixels are not coincident but are never more than 90 m apart.)

Although the $E_d(0^+)$ was obtained from an irradiance model, an uncalibrated zenith-viewing 256-channel spectroradiometer was used to monitor the hemispherical sky for variability caused by clouds. Because the airborne data were largely acquired under blue sky conditions, no retrieval improvement was found by using actual downwelling irradiance data. An infrared radiometer (Heimann KT-19 Radiation Thermometer) was used to concurrently measure sea surface temperature thus allow-

ing identification and interpretation of important oceanographic features such as the Gulf Stream western boundary.

B. Active (Laser) Data

The laser-induced fluorescence data were acquired with the AOL. The laser-induced fluorescence measurement methods were analogous to those already described.^{7,8,22} Briefly, 355-nm laser pulses are transmitted into the ocean to induce the broad spectrum CDOM fluorescence (~360–650 nm) and water Raman emission (~402 nm) from the surrounding water molecules.²² The resulting F/R ratio $F_{\text{CDOM}}(450)/R(402)$, is linearly related to the CDOM absorption coefficient^{16,19} and provides the truth data for comparison with the CDOM and detritus absorption coefficient retrieved from the upwelled radiances.⁹

Also, 532-nm laser pulses are transmitted vertically downward into the ocean to induce chlorophyll (and phycoerythrin fluorescence emission^{23,24}) from waterborne phytoplankton and water Raman emission from the surrounding seawater molecules. The concurrent chlorophyll (~670–690-nm) and phycoerythrin (~540–595-nm) fluorescence and water Raman spectral emissions (~645 nm) are collected by the same telespectroradiometer.

A spectral and radiometric calibration is also performed on the laser receiver radiometer before and after each flight mission by viewing the 0.75-m-diameter calibration sphere placed beneath the aircraft laser-viewing port. Because the laser receiver radiometer contains photomultiplier tubes (PMT's), additional steps are taken to maintain the calibration during flight. Immediately following the 0.75-m sphere calibration, a 10-cm-diameter calibration sphere within the AOL system is viewed by mechanically introducing (at the focal plane of the telescope) the radiation through fiber optics. The 10-cm sphere calibration is followed by viewing 40-ns pulsed radiation from a bank of red light-emitting diodes located behind the diffraction grating and in front of the fiber-optic face plate. The small calibration sphere allows immediate transfer of the 0.75-m sphere calibration into the aircraft domain at any time. The pulsed light-emitting diodes then provide transfer of the ground (and onboard) dc tungsten lamp calibrations to the wide bandwidth-pulsed portion of the AOL detection/amplification/digitization system. Calibration is maintained in flight by periodically viewing the 10-cm calibration sphere.

The original AOL system^{25–30} was recently modified to provide more complete rejection of the 532-nm laser excitation wavelength from the instrument spectrometer and substantial reduction of scattered light. Specifically, a narrow-band (notch) transmission filter was placed into the collimated segment of the light path and rejects considerable amounts of backscattered 532-nm radiation from the spectrometer. (The 532-nm pulse reflected from the notch filter is viewed by a PMT and is used to define the ocean surface target temporally and initiate digitization of

the fluorescence spectra.) Additional modifications include the removal of rigid light guides and all turning mirrors comprising the original optical axis. A fiber-optic face plate now occupies the focal plane of the new in-line optical path and transports the spectral radiation to mechanically reconfigured banks of original PMTs. The resolution of each of the 84 channels of the fiber-optic face plate system is ~ 4 nm. However, the number of PMT's currently available within the redesigned spectrometer is only 28, therefore groups of three fiber optical channels were optically combined at each PMT to achieve ~ 12 nm per output band for this experiment. The signal path from the PMT's through and including digitization remains essentially the same as reported previously.^{25–29} Compared with the original light guides, the fiber-optic channels have superior scattered-light rejection that is attributed to a considerably smaller viewing or acceptance angle.

5. Retrieval of Water-Leaving Radiances from At-Aircraft Oceanic Radiances

Although the flight altitude was only 150 m, reflected sky radiance and reflected path radiance must each be removed from the at-aircraft radiances. The reflected sky radiance correction is performed by selecting a measured sky radiance spectrum representing that portion of the sky being reflected into the down-looking spectroradiometer. Then 0.021 of this sky radiance³¹ is subtracted from all at-aircraft radiance spectra. The path radiance correction was developed from ocean radiance spectra acquired during passes conducted at altitudes of 150, 235, 300, and 320 m over a portion of the same water mass on the morning of 3 April 1995. The nominal amount of path radiance per meter of flight altitude determined from this earlier data set was applied to the data acquired over the entire flight line during the afternoon mission. To validate the atmospheric correction methodology, IOP retrievals were performed with radiance data acquired at several different altitudes during the morning mission. The results (not shown) demonstrated that these reflected sky and path radiance correction procedures were quite satisfactory.

6. Inherent Optical Property Retrieval Results

The inversion of the data model or **D** matrix² can be performed in several ways but we frequently use lower–upper triangular decomposition. If needed, singular value decomposition methods can also provide a quantitative evaluation of any suspected near singularities.³²

We used sensor bands that are near those of present and planned satellite sensors. The methodology is adapted easily to other band sets. The chosen bands (412, 490, 565-nm) allow one to (a) avoid the high variability of the phytoplankton absorption at 443 nm (because, in agreement with the research of others,³³ unpublished analyses of our airborne active–passive data suggest that the 443-nm band does not provide the best retrieval results), and (b)

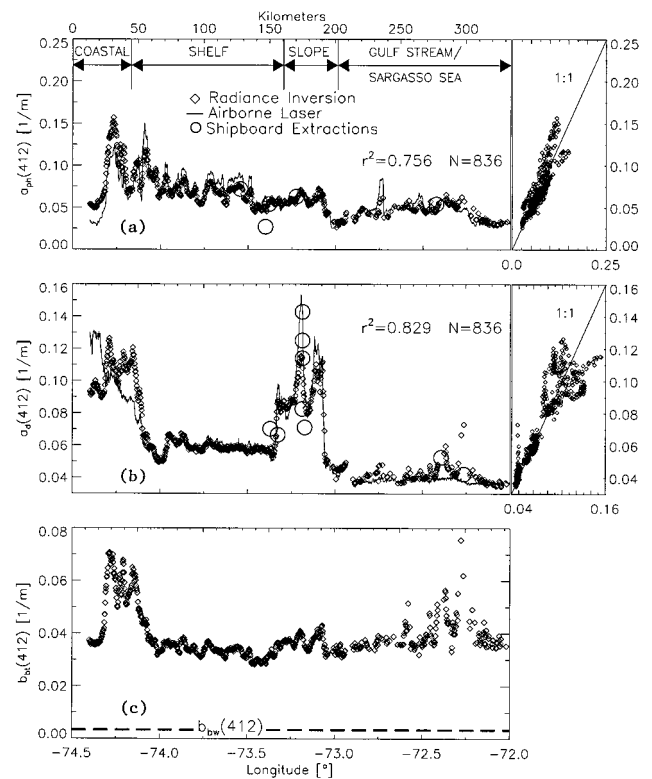


Fig. 2. (a) Along-track profile of phytoplankton absorption coefficient at 412 nm, $a_{ph}(412)$, retrieved from airborne water-leaving radiances plotted with chlorophyll absorption derived from concurrent airborne laser-induced F/R measurements obtained on the outbound portion of a flight to the Sargasso Sea during the afternoon of 3 April 1995. These parameters are also graphed as a scatterplot immediately to the right of the profile presentation. Limited absorption values derived from the supporting ship chlorophyll measurements are shown plotted as open circles. (b) Along-track profile of the CDOM and deritus absorption coefficient at 412 nm, $a_d(412)$, retrieved from the airborne water-leaving radiances plotted along with CDOM absorption measurements derived from airborne laser-induced CDOM F/R. These parameters are also graphed in the form of a scatterplot immediately to the right of the profile presentation. A limited number of supporting ship-derived CDOM absorption measurements are shown as open circles. (c) Along-track profile of the TCB coefficient, $b_{bt}(412)$, retrieved from the airborne water-leaving radiances. No truth data were available to validate the retrieved TCB.

employ the 565-nm band to avoid the phycoerythrobilin absorption near 545 nm (and provide further reduced CDOM and phytoplankton absorption relative to bands at ~ 550 nm). Use of the 490-nm band can carry a penalty of possible contamination from unmodeled phycourobilin absorption at 495 nm. Likewise, use of the 555-nm band radiances can potentially suffer from unmodeled phycoerythrobilin absorption. These latter two error sources are not considered serious but are undergoing evaluation.

The outbound southeast flight track of 3 April 1995 [Figs. 2(a)–2(c)] shows the inversion of the airborne water-leaving spectral radiance values plotted as open diamonds. The retrieved phytoplankton absorption coefficient [Fig. 2(a)] is compared with the absorption coefficients derived from the airborne

laser-induced chlorophyll F/R values shown as a solid curve. Also shown within Fig. 2(a) as open circles are chlorophyll absorption values derived from chlorophyll extraction measurements made from samples obtained by the R/V Cape Henlopen on 2 April, the day prior to the AOL flight. The open circles were used because of the rather busy appearance of the laser-derived and the model-retrieved phytoplankton absorption coefficient already present. The actual phytoplankton absorption value and its geographic position are located at the center of each circle. A specific absorption coefficient of $0.038 \text{ m}^{-1} \text{ mg m}^{-3}$ was used to convert the chlorophyll concentration measurements supplied by Rich Geider (University of Delaware) into units of absorption for direct comparison with the airborne remote-sensing data. A specific absorption coefficient of $0.038 \text{ m}^{-1} \text{ mg m}^{-3}$ is within published measurements of *in vivo* absorption by phytoplankton.³⁴ The retrieved phytoplankton absorption coefficient diverges from the 532-nm laser-determined absorption values as the track line approaches the coastal region at approximately 74.25°W longitude. Although the algorithm performs satisfactorily in Sargasso Sea, Gulf Stream, slope, and shelf waters, it is not yet satisfactory for use in coastal waters where unmodeled scatterers and absorbers may compromise the inversion accuracy. (No laser fluorescence data were obtained for a small section of the track line, around -72.8°W longitude.)

Similarly, the retrieved CDOM and detritus absorption coefficient [Fig. 2(b)] is compared with the airborne laser-derived CDOM absorption coefficients.¹⁹ Laboratory CDOM absorption measurements on samples acquired from the Cape Henlopen on the day prior to the remote-sensing flight are shown as open circles. These surface truthing CDOM measurements were supplied by Anthony Vodacek (University of Maryland). Familiar CDOM absorption signatures can be identified readily in Fig. 2(b). For example, the offshore decline of CDOM absorption is a central characteristic of the MAB.^{9,16,19,22} The radiance-retrieved midshelf values of $a_d(412)$ are consistent with other noncontemporaneous ship, aircraft, and satellite determinations of the CDOM absorption coefficient in the MAB.^{9,16,19} Another central characteristic of the CDOM absorption coefficient in the MAB is the abrupt decline at the Gulf Stream western boundary.^{9,16,19} During these experiments, the Gulf Stream western boundary was located at $\sim 73.1^\circ \text{W}$ longitude (as determined by the sea surface temperature measurements, not shown) near where the CDOM abruptly declines. The error in the CDOM and detritus retrieval around 74.25°W longitude is thought to be caused by errors in the estimated n exponent of the TCB spectral model. The empirical formula used to derive n does not work well for the combination of reflectances found within that particular segment.

In Fig. 2(c) no backscattering truth data were available to compare with the radiance-retrieved TCB coefficient. However, several features of the

along-track backscattering signature are notable. First, the backscattering is somewhat correlated with the phytoplankton particulates whose absorption is depicted in Fig. 2(a). Second, the backscattering is not highly correlated with the CDOM absorption which suggests, but does not prove, that (1) particulate detritus absorption does not dominate the CDOM absorption signature, and (2) use of a combined CDOM and detritus model is acceptable for this preliminary algorithm investigation. Finally, the total backscattering coefficients, $b_b(412) = b_{bt}(412) + b_{bw}(412)$, are nominally consistent with backscattering levels obtained by others.^{3-5,35} It should be emphasized that the backscattering must be concurrently retrieved, otherwise its contribution to the original radiances will be erroneously propagated into the phytoplankton and CDOM and detritus absorption coefficients.²

In Fig. 3 the retrieval results from the 20 April 1995 outbound track are shown. The phytoplankton absorption retrieval shown in Fig. 3(a) is compared with the absorption coefficients derived from the airborne laser chlorophyll F/R measurements. No surface truthing measurements were available for comparison with the remote-sensing data acquired during the 20 April mission. Note that in this data set the phytoplankton absorption coefficient retrieval is correlated with the laser-derived phytoplankton absorption coefficient within the coastal regime at $\sim 75.0^\circ \text{W}$ longitude. The retrieved CDOM and detritus absorption coefficient, $a_d(412)$ [Fig. 3(b)], is highly correlated with the 355-nm laser-derived CDOM absorption coefficient up to $\sim 74.75^\circ \text{W}$ longitude where the retrieval then falters within the coastal waters. The retrieved b_{bt} or TCB values [Fig. 3(c)] are consistent with those given in Fig. 2(c). (Within the segment around $\sim 73.0^\circ \text{W}$ longitude of Fig. 3 there was no usable data because uncorrectable reflectance from a single large cloud severely contaminated both the laser and the water-leaving radiance data. The cloud presence was validated by a sky-viewing spectroradiometer and by direct visual observation by at least two scientific team members. Also, the data near $\sim 72.1^\circ \text{W}$ longitude was removed because of cloud contamination as determined by visual observation and a sky-viewing spectroradiometer.)

Figure 4 shows the IOP retrievals for the 20 April 1995 inbound track on the return to Wallops Island. The phytoplankton absorption coefficient retrieval [Fig. 4(a)] is compared with the absorption coefficients derived from the airborne laser F/R values. The correlation of subtle features between the retrieved phytoplankton absorption coefficient and the F/R truth data can be seen. The $a_d(412)$ absorption coefficient and the CDOM absorption coefficient laser truth data show similar agreement and correlations. Again, no backscattering truth data were available, but the TCB retrievals in Fig. 4(c) are within the expected nominal range. (Missing data segments near $\sim 73.0^\circ \text{W}$ longitude and $\sim 72.1^\circ \text{W}$ longitude in

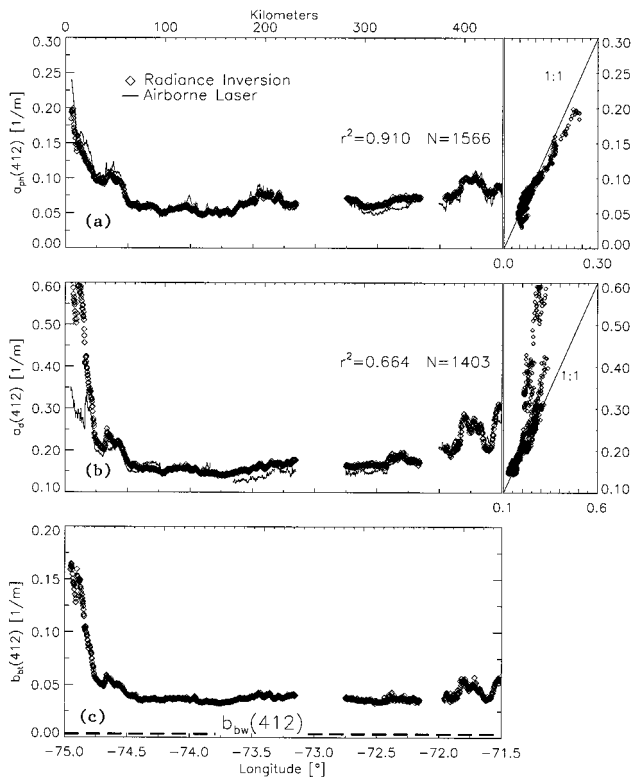


Fig. 3. (a) Along-track profile of phytoplankton absorption coefficient at 412 nm retrieved from airborne water-leaving radiances plotted with chlorophyll absorption derived from concurrent airborne laser-induced F/R measurements obtained on the outbound portion of a flight flown between Wallops Island, Virginia, and Block Island, Rhode Island, on 20 April 1995. These parameters are also graphed in the form of a scatterplot immediately to the right of the profile presentation. (b) Along-track profile of the CDOM and detritus absorption coefficient at 412 nm concurrently retrieved from the airborne water-leaving radiances is plotted along with CDOM absorption measurements derived from airborne laser-induced CDOM F/R. (c) Along-track profile of the TCB coefficient retrieved from the airborne water-leaving radiances. No truth data were available to validate the retrieved TCB. Note that the vertical scale for b_{bt} in (c) is different from (a) and (b). The blank portions of the track line at $\sim 72.3^\circ$ W longitude and $\sim 72.1^\circ$ W longitude denote lost data because of cloud contamination.

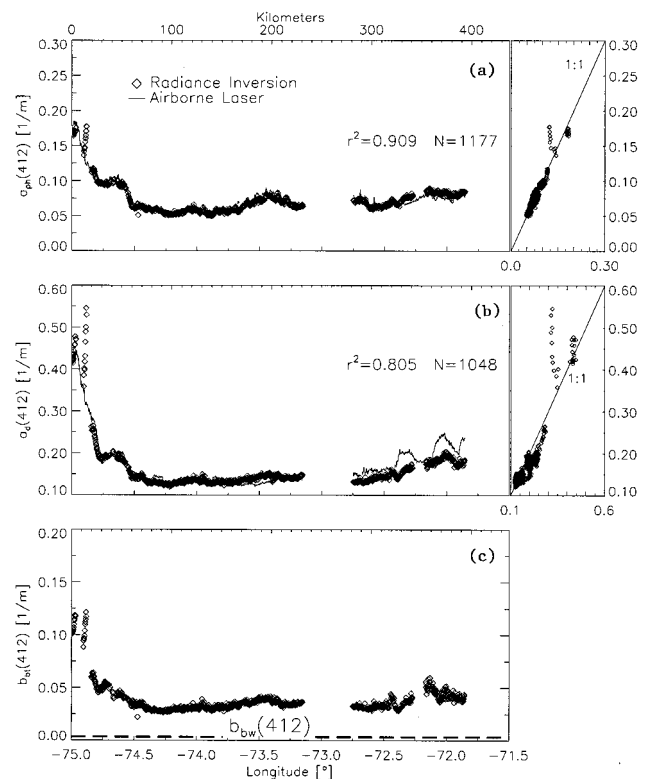


Fig. 4. (a) Along-track profile of phytoplankton absorption coefficient at 412 nm retrieved from airborne water-leaving radiances plotted with chlorophyll absorption derived from concurrent airborne laser-induced F/R measurements obtained on the inbound portion of a flight flown between Wallops Island, Virginia, and Block Island, Rhode Island, on 20 April 1995. These parameters are also graphed in the form of a scatterplot immediately to the right of the profile presentation. (b) Along-track profile of the CDOM and detritus absorption coefficient at 412 nm concurrently retrieved from the airborne water-leaving radiances plotted along with CDOM absorption measurements derived from airborne laser-induced CDOM F/R. (c) Along-track profile of the TCB coefficient retrieved from the airborne water-leaving radiances. No truth data were available to validate the retrieved TCB. Note that the vertical scale for b_{bt} in (c) is different from (a) and (b). The portions of the track line at $\sim 72.3^\circ$ W longitude and $\sim 72.1^\circ$ W longitude denote lost data because of cloud contamination.

Fig. 4 were caused by the same cloud contamination discussed in Fig. 3.)

7. Discussion

A previously published radiance model inversion theory has been successfully tested by using airborne water-leaving radiances to retrieve the CDOM and detritus absorption coefficient, the phytoplankton absorption coefficient, and the total backscattering coefficient. Linear matrix inversion of water-leaving spectral radiances was found to perform satisfactorily using airborne water-leaving radiance spectra even in the presence of instrument-induced noise. Previous investigations with the inversion methodology used simulated radiance spectra containing no noise from instrument or environmental sources.²

Laser-induced fluorescence from CDOM and phytoplankton chlorophyll were utilized together with concurrent ocean color radiance spectra to test the model inversion methodology for retrieval of the three most dominant IOP's: phytoplankton absorption, CDOM and detritus absorption, and TCB absorption. A modest amount of supporting chlorophyll and CDOM data derived from ship samples were shown for one of the data sets used in this initial application of the model inversion methodology. The strength of the airborne laser-derived IOP truth data lies in the large volume of the concurrent active-passive paired observations coupled with the diversity of oceanographic provinces traversed during airborne experiments. Previously, airborne chlorophyll and CDOM fluorescence data had been directed primarily toward support of major field experiments,^{7-9,11-15} forward

modeling of water-leaving radiances,⁸ and CDOM variability mapping.^{9,22}

The backscattering wavelength ratio model requires a variable exponent to provide the best IOP retrieval. The value of n affects the retrieval of the CDOM absorption coefficient more than the retrieval of the phytoplankton absorption coefficient.² Therefore large errors in the CDOM and detritus retrieval can be expected if n is not correct. It is recommended that data from different oceanographic regions and seasons be acquired to compile a more reliable lookup table for a general set of a_1 and a_2 parameters used to derive n . The availability of backscattering truth data would allow further improvements to the existing model. Accordingly, we recommend that more attention be paid to this important parameter.^{36–38} Although shipboard backscattering instrumentation is becoming more available,³ the data density is still too sparse to be of any real utility for general application to different water masses. We consider knowledge of TCB to be fundamental to NASA's satellite algorithm development programs. Because there continues to be a paucity of backscattering data from ship cruises, we recommend the development of an airborne laser backscattering measurement capability. Two-channel crossed-polarization lidar systems show much promise for airborne retrieval of the total scattering coefficient, but such sensors are not yet ready for routine use.

The spatial variability of the TCB [Figs. 2(c), 3(c), and 4(c)] emphasizes the importance of including it in the retrieval computational process. Had the TCB not been solved for in the 3-band retrieval, then it must by necessity be constrained by a model (or, worse yet, a fixed constant) within a 2-band matrix retrieval. For a fixed-constant backscattering model (e.g., within a 2×2 matrix inversion), the observed backscattering variability [Figs. 2(c), 3(c), and 4(c)] would be erroneously propagated into the phytoplankton and CDOM absorption coefficient retrievals.

The 443-nm band consistently gave poorer results than the 490-nm band when used in combination with the 412- and 565-nm bands. This suggests that it is important to avoid choosing sensor band locations within spectral regions having naturally elevated absorption and backscattering variability. In addition, we found by independent model inversion studies that the retrieval errors for all the IOP's are rather strongly dependent on the phytoplankton Gaussian spectral model. Retrieval errors are thus exacerbated by the natural spectral variability³⁹ of phytoplankton absorption. By choosing a single Gaussian phytoplankton spectral model³⁹ as done here, IOP errors are likely but can be minimized by avoiding spectral regions of high variability.

The CDOM absorption levels in the MAB are higher by $\sim 2\times$ than found in the Southern California Bight²² and the western coast of Florida just outside Tampa Bay and $\sim 3\times$ higher than waters outside Monterey Bay, California.¹⁹ Simulated model inversions have shown that the inversion process func-

tions satisfactorily for $a_d(355)$ levels² through $\sim 1.0 \text{ m}^{-1}$. Thus reasonably accurate retrievals should be expected over wide areas of the ocean. Also, chlorophyll levels during these algorithm development field experiments were no greater than $\sim 4\text{--}5 \text{ mg/m}^3$. However, simulated model inversions suggest that the algorithm will continue to operate in much higher ($\sim 20\text{--}30 \text{ mg/m}^3$) phytoplankton absorption regimes.² Forward modeling using water-leaving radiances and ship-validated chlorophyll concentrations of $0.7\text{--}27 \text{ mg/m}^3$ further suggests that the inversion will perform in a satisfactory manner in high-chlorophyll regions.⁸ The mathematical inversion process will operate over a wide range of IOP's with little chance of singularity, but the user must be alert because even-determined solutions may return physically unacceptable solutions (such as negative IOP's) when inaccurate data or model parameters are used.² Of course these conditions are easily flagged during the inversion computations.

This initial field application of the model inversion methodology worked well in shelf, slope, Gulf Stream, and Sargasso Sea water masses but not consistently in the coastal waters. The algorithm remains preliminary pending tests in other oceanic provinces and comparison with additional airborne laser-induced fluorescence data sets with supporting surface truth measurements. The application of the model inversion methodology to coastal waters will require additional refinements to the technique.

Appendix A: Nomenclature

a_d	Absorption coefficient of CDOM and detritus (m^{-1});
a_{ph}	absorption coefficient of phytoplankton particles (m^{-1});
a_w	absorption coefficient of water (m^{-1});
b_b	total backscattering coefficient (m^{-1}); $b_b = b_{\text{bw}} + b_{\text{bt}}$;
b_{bt}	TCB coefficient (m^{-1});
b_{bw}	backscattering of seawater (m^{-1});
D	data and model matrix;
F/R	chlorophyll-fluorescence/water Raman ratio for airborne laser data;
g	phytoplankton Gaussian model spectral width parameter (nm);
h	$-(a_w + b_{\text{bw}}v)$; vector of hydrospheric constants and water-leaving radiances;
N	number of samples used in regression or along-track profile;
n	total constituent backscattering spectral model exponent;
p	oceanic state vector of retrieved IOP's at their reference wavelengths;
S	spectral slope for the a_d model;
v	$(1 - 1/X)$ (dimensionless);
X	$b_b/(b_b + a)$ (dimensionless);
λ	wavelength (nm);
λ_b	reference wavelength for TCB (nm);
λ_d	reference wavelength for CDOM and detritus absorption (nm);

- λ_g peak wavelength for Gaussian phytoplankton absorption model (nm);
 λ_i wavelength of observational bands, $i = 1, 2, 3$.

The continued support and encouragement of the NASA Ocean Biology Program is gratefully acknowledged. We are very appreciative of the extracted chlorophyll fluorescence measurements provided by Rich Geider (University of Delaware) and the CDOM absorption measurements given by Anthony Vodacek (University of Maryland).

References

- H. R. Gordon, D. K. Clark, J. W. Brown, O. B. Brown, R. H. Evans, and W. W. Broenkow, "Phytoplankton pigment concentrations in the Middle Atlantic Bight: comparison between ship determinations and the coastal zone color scanner estimates," *Appl. Opt.* **22**, 20–36 (1983).
- F. E. Hoge and P. E. Lyon, "Satellite retrieval of inherent optical properties by linear matrix inversion of oceanic radiance models: an analysis of model and radiance measurement errors," *J. Geophys. Res.* **101**, 16,631–16,648 (1996).
- R. A. Maffione and D. R. Dana, "Instruments and methods for measuring the backward-scattering coefficient of ocean waters," *Appl. Opt.* **36**, 6057–6067 (1997).
- R. A. Maffione, D. R. Dana, and R. C. Honey, "Instrument for underwater measurement of optical backscatter," in *Underwater Imaging, Photography, and Visibility*, R. W. Spinrad, ed., Proc. SPIE **1537**, 173–184 (1991).
- J. H. Smart, "Empirical relationships between optical properties in the ocean," in *Ocean Optics XI*, G. D. Gilbert, ed., Proc. SPIE **1750**, 276–298 (1992).
- R. A. Maffione, D. R. Dana, and J. M. Voss, "Spectral dependence of optical backscattering in the ocean," presented at OSA Annual Meeting, Portland, Ore., 10–15 September 1995, Paper MDD4, p. 57.
- F. E. Hoge and R. N. Swift, "The influence of chlorophyll pigment upon upwelling spectral radiances from the north Atlantic Ocean: an active-passive correlation spectroscopy study," *Deep Sea Res.* **40**, 265–277 (1993).
- F. E. Hoge, R. N. Swift, and J. K. Yungel, "Oceanic radiance model development and validation: application of airborne active-passive ocean color spectral measurements," *Appl. Opt.* **34**, 3468–3476 (1995).
- F. E. Hoge, M. E. Williams, R. N. Swift, J. K. Yungel, and A. Vodacek, "Satellite retrieval of the absorption coefficient of chromophoric dissolved organic matter in continental margins," *J. Geophys. Res.* **100**, 24,847–24,854 (1995).
- M. P. F. Bristow, D. Nielsen, D. Bundy, and F. Furtek, "Use of water-Raman emission to correct airborne laser fluorosensor data for effects of water optical attenuation," *Appl. Opt.* **20**, 2889–2906 (1981).
- R. C. Smith, O. B. Brown, F. E. Hoge, K. S. Baker, R. H. Evans, R. N. Swift, and W. E. Esaias, "Multiplatform sampling (ship, aircraft, and satellite) of a Gulf Stream warm core ring," *Appl. Opt.* **26**, 2068–2081 (1987).
- J. W. Campbell and W. E. Esaias, "Spatial patterns in temperature and chlorophyll on Nantucket Shoals from airborne remote sensing data, May 7–9, 1981," *J. Mar. Res.* **43**, 139–161 (1985).
- J. W. Campbell and W. E. Esaias, "Basis for spectral curvature algorithms in remote sensing of chlorophyll," *Appl. Opt.* **22**, 1084–1093 (1983).
- J. J. Walsh, C. D. Wirick, L. J. Pietrafesa, T. E. Whitledge, F. E. Hoge, and R. N. Swift, "High-frequency sampling of the 1984 spring bloom within the Mid-Atlantic Bight: synoptic shipboard, aircraft, and in situ perspectives of the SEEP-I Experiment," *Cont. Shelf Res.* **8**, 529–563 (1988).
- J. Martin, et al., "Testing the iron hypothesis in ecosystems of the equatorial Pacific Ocean," *Nature (London)* **371**, 123–129 (1994).
- F. E. Hoge, A. Vodacek, and N. V. Blough, "Inherent optical properties of the ocean: retrieval of the absorption coefficient of chromophoric dissolved organic matter from fluorescence measurements," *Limnol. Oceanogr.* **38**, 1394–1402 (1993).
- G. M. Ferrari and S. Tassan, "On the accuracy of determining light absorption by 'yellow substance' through measurements of induced fluorescence," *Limnol. Oceanogr.* **36**, 777–786 (1991).
- G. M. Ferrari, M. D. Dowell, S. Grossi, and C. Targa, "Relationship between the optical properties of chromophoric dissolved organic matter and total concentration of dissolved organic carbon in the southern Baltic Sea region," *Mar. Chem.* **55**, 299–316 (1996).
- F. E. Hoge, A. Vodacek, R. N. Swift, J. K. Yungel, and N. V. Blough, "Inherent optical properties of the ocean: retrieval of the absorption coefficient of chromophoric dissolved organic matter from airborne laser spectral fluorescence measurements," *Appl. Opt.* **34**, 7032–7038 (1995).
- W. A. Hovis and J. S. Knoll, "Characteristics of an internally illuminated calibration sphere," *Appl. Opt.* **22**, 4004–4007 (1983).
- J. L. Mueller, "The second SeaWiFS intercalibration round-robin experiment, SIRREX-2, June 1993," NASA Tech. Memo. 104566, S. B. Hooker and E. R. Firestone, eds. (NASA Goddard Space Flight Center, Greenbelt, Md., 1994), Vol. 16.
- F. E. Hoge, R. N. Swift, J. K. Yungel, and A. Vodacek, "Fluorescence of dissolved organic matter: a comparison of North Pacific and North Atlantic Oceans during April 1991," *J. Geophys. Res.* **98**, 22,779–22,787 (1993).
- F. E. Hoge and R. N. Swift, "Active-passive correlation spectroscopy: a new technique for identifying ocean color algorithm spectral regions," *Appl. Opt.* **25**, 2571–2583 (1986).
- F. E. Hoge and R. N. Swift, "Phytoplankton accessory pigments: evidence for the influence of phycoerythrin on the submarine light field," *Remote Sensing Environ.* **34**, 19–25 (1990).
- F. E. Hoge and R. N. Swift, "Oil film thickness measurement using airborne laser-induced water Raman backscatter," *Appl. Opt.* **19**, 3269–3281 (1980).
- F. E. Hoge and R. N. Swift, "Airborne simultaneous spectroscopic detection of laser-induced water Raman backscatter and fluorescence from chlorophyll *a* and other naturally occurring pigments," *Appl. Opt.* **20**, 3197–3205 (1981).
- F. E. Hoge and R. N. Swift, "Airborne dual laser excitation and mapping of phytoplankton photopigments in a Gulf Stream warm core ring," *Appl. Opt.* **22**, 2272–2281 (1983).
- F. E. Hoge and R. N. Swift, "Airborne detection of oceanic turbidity cell structure using depth-resolved laser-induced water Raman backscatter," *Appl. Opt.* **22**, 3778–3786 (1983).
- F. E. Hoge, R. E. Berry, and R. N. Swift, "Active-passive airborne ocean color measurement: 1. Instrumentation," *Appl. Opt.* **25**, 39–47 (1986).
- F. E. Hoge, R. N. Swift, and J. K. Yungel, "Active-passive airborne ocean color measurement: 2. Applications," *Appl. Opt.* **25**, 48–57 (1986).
- H. R. Gordon, O. B. Brown, R. H. Evans, J. W. Brown, R. C. Smith, K. S. Baker, and D. K. Clark, "A semianalytic radiance model of ocean color," *J. Geophys. Res.* **93**, 10,909–10,924 (1988).
- W. H. Press, S. A. Teukolsky, W. T. Vetterling, and B. P. Flannery, *Numerical Recipes in Fortran*, 2nd ed. (Cambridge U. Press, Port Chester, N.Y., 1992).

33. J. Aiken, G. F. Moore, C. C. Trees, S. B. Hooker, and D. K. Clark, "The SeaWiFS CZCS-type pigment algorithm," NASA Tech. Memo. 104566, S. B. Hooker and E. R. Firestone, eds. (NASA Goddard Space Flight Center, Greenbelt, Md., 1995), Vol. 29.
34. S. Sathyendranath, L. Lazzara, and L. Prieur, "Variations in the spectral values of the specific absorption of phytoplankton," *Limnol. Oceanogr.* **32**, 403–415 (1987).
35. C. S. Roesler and M. J. Perry, "In situ phytoplankton absorption, fluorescence emission, and particulate backscattering spectra determined from reflectance," *J. Geophys. Res.* **100**, 13,279–13,294 (1995).
36. Z. P. Lee, K. L. Carder, S. K. Hawes, R. G. Steward, T. G. Peacock, and C. O. Davis, "Model for the interpretation of hyperspectral remote-sensing reflectance," *Appl. Opt.* **33**, 5721–5732 (1994).
37. A. D. Weideman, R. H. Stavn, J. R. V. Zanefeld, and M. R. Wilcox, "Error in predicting hydrosol backscattering from remotely sensed reflectance," *J. Geophys. Res.* **100**, 13,163–13,177 (1995).
38. C. S. Roesler and M. J. Perry, "In situ phytoplankton absorption, fluorescence emission, and particulate backscattering spectra determined from reflectance," *J. Geophys. Res.* **100**, 13,279–13,294 (1995).
39. N. Hoepffner and S. Sathyendranath, "Determination of the major groups of phytoplankton pigments from the absorption spectra of total particulate matter," *J. Geophys. Res.* **98**, 22,789–22,803 (1993).